Evolution of a lidar network for tropospheric aerosol detection in East Asia

Atsushi Shimizu
Tomoaki Nishizawa
Yoshitaka Jin
Sang-Woo Kim
Zifa Wang
Dashdondog Batdorj
Nobuo Sugimoto

SPIE.

Evolution of a lidar network for tropospheric aerosol detection in East Asia

Atsushi Shimizu,[a,*] **Tomoaki Nishizawa,**[a] **Yoshitaka Jin,**[a] **Sang-Woo Kim,**[b] **Zifa Wang,**[c] **Dashdondog Batdorj,**[d] **and Nobuo Sugimoto**[a]

[a]National Institute for Environmental Studies, 16-2 Onogawa, Tsukuba, Ibaraki 305-8506, Japan
[b]Seoul National University, 1 Gwanak-ro, Gwanak-gu, Seoul 08826, Republic of Korea
[c]Chinese Academy of Sciences, Institute of Atmospheric Physics, Chao Yang District, Beijing 100029, China
[d]National Agency for Meteorology and Environmental Monitoring, Juulchny, Guidamj-5, Ulaanbaatar-46 210646, Mongolia

Abstract. A regional elastic-scattering lidar network called Asian dust and aerosol lidar observation network (AD-Net) has operated for 15 years (since 2001) in East Asia. In this network, the extinction coefficient of aerosols below an altitude of 9 km is continuously obtained when conditions are clear; the coefficient is divided into two parts: dust extinction and spherical extinction coefficients. The dust extinction coefficient has been compared with several parameters measured by other instruments and utilized by various studies, including studies on the epidemiology of Asian dust. Recent expansion of the lidar system at some observatories allows more optical parameters to be retrieved at those observatories. All AD-Net products are used for monitoring global environmental change as an activity of global atmospheric watch lidar observation network. © *The Authors. Published by SPIE under a Creative Commons Attribution 3.0 Unported License. Distribution or reproduction of this work in whole or in part requires full attribution of the original publication, including its DOI.* [DOI: 10.1117/1.OE.56.3.031219]

1 Introduction

Aerosols, i.e., particulate matter (PM) in the atmosphere, play a key role in radiation transfer in the Earth system. Aerosols scatter or absorb sunlight, thereby cooling or heating atmospheric layers. Individual aerosol particles also act as condensation nuclei or ice nuclei in the troposphere. Therefore, knowledge of the location and optical properties of aerosols is crucial for understanding the thermal balance of the atmosphere.[1]

In addition, PM near the Earth's surface is a known risk factor for human health. The International Agency for Research on Cancer has classified PM as a high-level risk factor for lung cancer and other cancers.[2] Thus, PM near the Earth's surface is one of the most important properties of the ambient atmospheric environment that should be monitored.

The most powerful remote sensing technique to determine the vertical distribution of an aerosol layer in near real time is light detection and ranging (lidar). Although a precipitation radar can cover a horizontal area several hundred kilometers in diameter, lidar can measure the aerosol distribution just above the lidar instrument, or of around several kilometers, even if the lidar instrument has a horizontal scanning mechanism. Thus, to understand the three-dimensional distribution of aerosols on a regional scale, a lidar network is indispensable. Several lidar networks have already been constructed. For example, the European Aerosol Research Lidar Network (EARLINET), which has stations in Europe, was established in 2000.[3] Lidars in EARLINET are organized to observe atmosphere in the region synchronously, and their data quality is assured for research activities related to the radiative forcing. In East Asia, the National Institute for Environmental Studies (NIES), Japan, has developed a network of lidar instruments called Asian dust and aerosol lidar observation network (AD-Net), which is a collaborative project of many universities, institutes, and national and local governments. Although AD-Net was initially established to monitor the transportation of Asian dust, anthropogenic particles are another important target in these days. Micropulse Lidar Network (MPLNET)[4] led by NASA (National Aeronautics and Space Administration) has the widest geographical distribution of lidars in the world, from the equatorial to the polar regions, and has a close relation to AERONET (NASA Aerosol Robotic Network). Latin American Lidar Network (LALINET aka ALINE)[5] was established to study the climatology of aerosols and is also devoted to the early warning of volcanic eruptions. Although each network has its original strategy fitting technical bases and location, these lidar networks contribute to GALION (GAW Aerosol Lidar Observation Network) for monitoring of the atmospheric conditions around the globe.

In this paper, we describe the historical and current status of AD-Net along with the hardware specifications of the lidar systems and the data processing method, and we present examples of the application of lidar data. We also introduce the new generation of lidar equipment and techniques used in AD-Net. Finally, we review the future outlook of this ground-based lidar network.

2 Elastic-Scattering Lidar in AD-Net

2.1 History of AD-Net and Station Locations

In 1996, NIES, in Tsukuba, Japan, developed an automated elastic scattering lidar (EL) system that could operate continuously without human intervention. At that time, only

the total backscatter signal intensity at 532 nm (I_{532}) was recorded, and only aerosols and cloud layers could be identified. In 1999, the system was modified so that the polarization state of the backscattered light could also be recorded, allowing aerosol particle shapes to be investigated. By this modification, the NIES automated lidar system acquired the capability to distinguish mineral dust particles from anthropogenic particles and ice particles in cirrus clouds from water droplets in convective clouds. In 2001, an initial lidar network was constructed for the ACE-Asia campaign,[6] an important aim of which was to investigate the distribution of Asian dust. For ACE-Asia, NIES operated lidar observatories at Tsukuba, Nagasaki, and Beijing and collaborated with other lidar observatories in Japan.[7,8] Since then, the number of NIES-type lidar observatories, which follow a mostly uniform operational strategy, has increased; at present, AD-Net comprises a total of 20 observatories in East Asia (i.e., in Japan, Korea, China, and Mongolia). Figure 1 shows the locations of AD-Net lidar observatories in operation as of July 2016. Nowadays some lidars were modified to Raman lidar (RL) or multiwavelength Raman lidar (MRL) systems (see Sec. 3). However, the data treatment for elastic scattering channels of such lidars is the same as that for EL. Thus, we describe EL system at first (Sec. 2.2) and then introduce the common data processing procedures on elastic scattering channels in Sec. 2.3.

2.2 Hardware of an Elastic-Scattering Lidar System

The fundamental and common information about aerosol is retrieved from elastic scattering channels in all types of AD-Net lidars. Here, the specifications and configuration of the AD-Net elastic lidar (EL) system are described.

Table 1 and Fig. 2(a) summarize the specs and configurations of EL. The EL employs a flashlamp-pumped Q-switching Nd:YAG laser as the light source. Pulsed light is emitted with a fundamental wavelength of 1064 nm and a second harmonic of 532 nm, produced by second harmonics generation. A pulse with a mean power of 50 mJ (sum of 20 mJ at 1064 nm and 30 mJ at 532 nm) and a duration of 8 ns is expanded by a beam expander and emitted at a frequency of 10 Hz in the direction of the zenith. Backscattered light from the atmosphere is collected by a Schmidt–Cassegrain telescope with a diameter of 20 cm

Fig. 1 Locations of current AD-Net lidar observatories. Green, red, and blue symbols indicate locations of EL, RL, MRL systems, respectively.

and a field of view of 1 mrad and separated by a dichroic mirror into P_{1064} (light intensity at 1064 nm) and P_{532} (light intensity at 532 nm). Then, P_{532} is further separated by a beam splitter cube into two components: P_{532p} (the polarizing angle is parallel to that of the emitted laser beam) and P_{532s} (the polarizing angle is perpendicular). The extinction ratio of the beam splitter cube is 0.001. P_{532p} and P_{532s} are both detected by photomultiplier tubes (PMTs), and P_{1064} is detected by an avalanche photodiode. Signal intensities are sampled at 25 MHz (corresponding to a range resolution of 6 m), digitized with 12- or 16-bit AD converters, and recorded by a personal computer as vertical profiles $P_{532p}(z)$, $P_{532s}(z)$, and $P_{1064}(z)$, where z denotes the altitude above the lidar. To obtain a high signal-to-noise ratio, signals are accumulated for 5 min (i.e., 3000 laser shots). To reduce the flashlamp consumption, a 10-min rest period follows each 5-min emission period. Thus, the system obtains four profiles each hour.

The lidar system is installed in a room with a glass window in the roof. Because the observations are made through the glass, the system can be operated in all weather conditions, including rain and snow. Every hour, the observation results are transferred to an NIES data server via the Internet, the condition of the lidar system is checked, and an initial analysis is performed. An exception is the Beijing lidar, which by Chinese law is not allowed to send data to NIES in real time.

2.3 Data Processing

To obtain the optical properties of aerosols, the following analyses are applied to the AD-Net observation results in elastic-scattering channels of EL, RL, and MRL.

The background removed and range corrected signal intensities of the three channels (I_{532p}, I_{532s}, and I_{1064}) must be calibrated before physical quantities such as the attenuated backscatter coefficient can be determined. First, total backscatter intensity I_{532} is calculated as

$$I_{532} = I_{532p} + \mathrm{Cd} \times I_{532s}, \qquad (1)$$

where Cd is the ratio of sensitivities between the two PMTs used to detect the parallel and perpendicular components (see Sec. 2.2). Once I_{532} has been obtained, a frequency histogram of all $I_{532}(z,t)$ in the height range of 1200 to 6000 m is constructed. The histogram peak corresponds empirically to the system calibration constant (C_{532}) because the molecular backscatter is dominant in this height range with lighter aerosol loading conditions. Then, the attenuated backscatter coefficient at 532 nm (β'_{532}) is estimated as the product of C_{532} and I_{532}, and the volume linear depolarization ratio (δv_{532}), defined as

$$\delta v_{532} = \mathrm{Cd} \times I_{532s}/I_{532p}, \qquad (2)$$

is also calculated. Next, the intensity of the 1064 nm signal is calibrated using the ratio of sensitivities at β'_{532} and β'_{1064}. Near the bottom of water clouds, the backscatter coefficient does not have a strong dependency on wavelength because the scatterers are large (radius is usually >10 μm) compared with the wavelength of the laser light. Thus, the calibration constant for 1064 nm (C_{1064}) can be determined from β'_{532} and β'_{1064}. In this calculation, we ignore the difference in

Table 1 Specifications of the AD-Net lidars.

Lidar type	EL and RL	MRL	RHL
Transmitter			
Laser	Nd:YAG, linearly polarized, (Quantel, Brilliant Ultra)	Nd:YAG, linearly polarized, (Quantel, Brilliant Easy)	Nd:YAG, linearly polarized, injection-seeded, (Continuum, Surelite I)
Wavelength (nm)	1064, 532	1064, 532, 355	1064, 532, 355
Pulse energy	20 mJ for 1064 nm, 30 mJ for 532 nm	110, 110, 50 mJ for 1064, 532, 355 nm	100 mJ for each wavelength
Repetition rate		10 Hz	
Receiver			
Telescope	Schmidt–Cassegrain, Dia. = 20 cm (Celestron, C8-AXLT)	Schmidt–Cassegrain, Dia. = 20 cm (Celestron, C8-AXLT)	Cassegrain, Dia. = 21 cm (Takahashi, CN-212)
FOV		1mrad	
Band-path filter		1 nm for each wavelength	
Detectors	• APD (Licel, APD-1.5) for 1064 nm	• APD (Licel, APD-1.5) for 1064 nm	• APD (Licel, APD-1.5) for 1064 nm
	• PMT (Hamamatsu, H7421-40) or PMT (Licel, PM-HV-20) for 607 nm*	• PMT (Licel, R9880-20) for 607 nm	• PMTs (Licel, PM-HV-20) for 532 nm
	• PMTs (Hamamatsu, H6780-02) for 532 nm	• PMTs (Licel, R9880-110) for 532, 387, 355 nm	• PMTs (Licel, PM-HV-03) for 387, 355 nm
Data acquisition			
	• A/D converter: 25 MHz, 12 or 16 bit (Turtle Industry) for 1064, 532 nm	• A/D converter: 25 MHz, 16 bit (Turtle Industry) for 1064, 532, 355 nm	• A/D converter: 40 MHz, 12 (Licel) for 1064, 532, 355 nm
	• Photon counter: 100 MHz count rate (SigmaSpace) or 250 MHz count rate (Licel) for 607 nm*	• Photon counter: 250 MHz count rate (Licel) for 607, 387 nm	• Photon counter: 250 MHz count rate (Licel) for 387 nm

aerosol optical depth at 532 and 1064 nm between the surface and the cloud base because the aerosol loading is not expected to be very high in that interval. Once C_{1064} has been determined, the attenuated backscatter coefficient at 1064 nm (β'_{1064}) is calculated as the product of C_{1064} and I_{1064}. β'_{532}, δv_{532}, and β'_{1064} are each averaged over five vertical points to increase the signal-to-noise ratio (which reduces the height resolution to 30 m). Examples of time–height sections of these quantities are shown in Fig. 3, and the calibration procedure is summarized in Fig. 4.

The depolarization ratio, a measure of the irregularity of the scatterer shape,[9] is the most important property of Asian dust measured by lidar systems. To calculate the depolarization ratio, it is important to first calibrate the signal intensities of the I_{532p} and I_{532s} channels. In AD-Net, the difference in sensitivity between the two PMTs used to detect these components is checked routinely by the following method. A sheet polarizer whose polarizing direction is set at 45 deg to the polarizing plane of emitted light is inserted in front of the beam splitter cube, and the backscatter signal from

the sky is recorded as a reference signal. In this reference record, the light intensities of the two channels are equal after the sheet polarizer, so the calibration constant Cd can be obtained by comparing the recorded values of I_{532p} and I_{532s}. Next, the sheet polarizer is rotated 90 deg to set the polarizing angle at −45 deg, and another reference signal is recorded. This pair of reference signals reduces any error caused by poor positioning of the sheet polarizer.[10] The reference signals are usually recorded once per year for each lidar.

The cloud base height must be determined first because the aerosol layer analysis cannot be applied to cloud layers. In AD-Net, the cloud base height is determined from the vertical gradient of β'_{1064} and the peak value of β'_{1064} between the cloud base and the apparent cloud top, where β'_{1064} is equal to that of the cloud base. The threshold values are determined empirically because they depend on the vertical resolution and signal accumulation time of the lidar measurements and there are no true cloud base height reference data with equivalent lidar time and height resolutions at each observatory. Therefore,
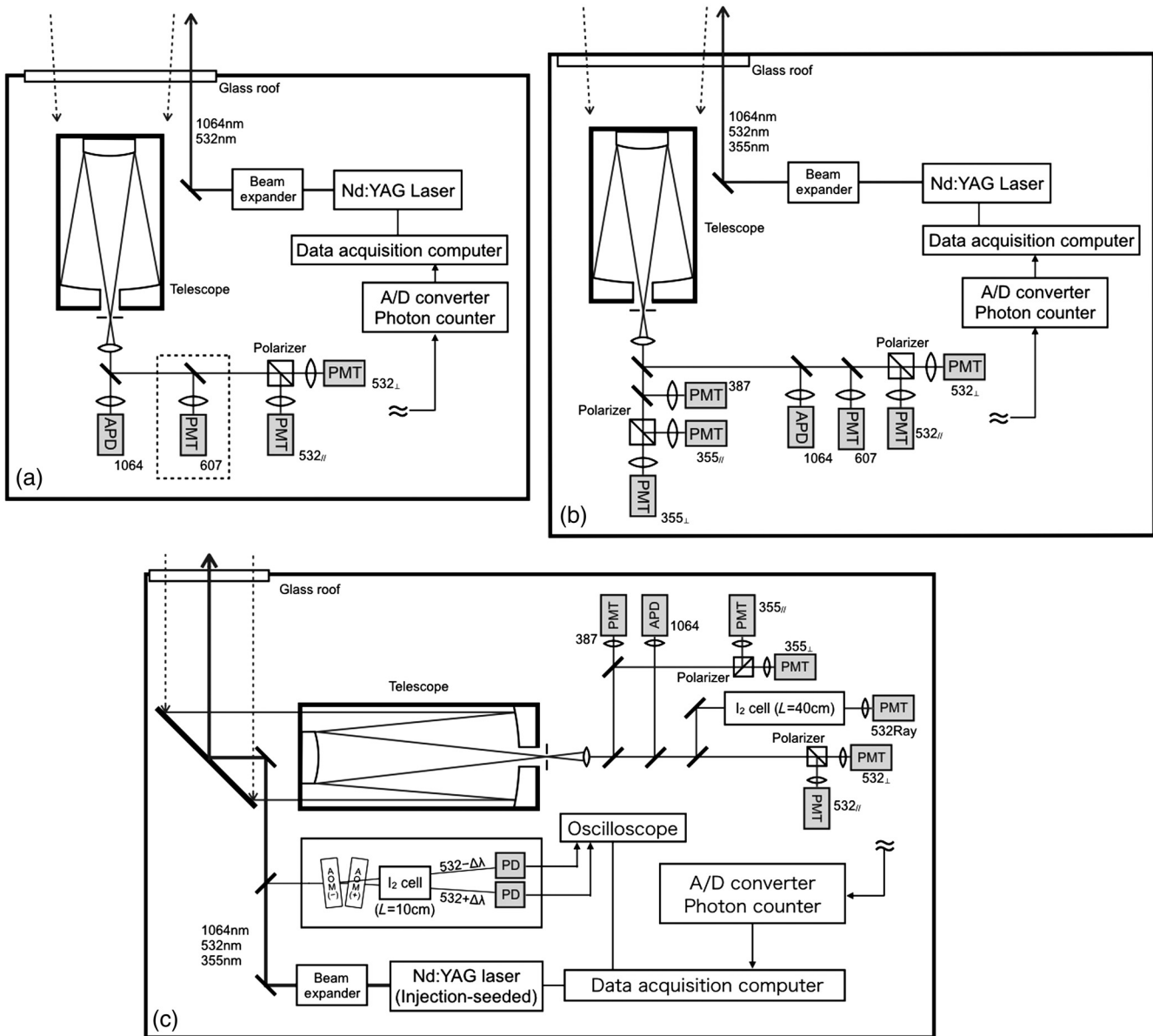
Fig. 2 Configurations of the lidars used in AD-Net. (a) EL and RL, (b) MRL, and (c) RHL.

the thresholds are determined subjectively by estimating the cloud distribution on time–height sections [see Figs. 3(d) and 3(e)].

Scattering by rain droplets or snowflakes obscures the signal from aerosols. Thus, data recorded during rainy or snowy conditions must be eliminated before the analysis. Moreover, the affected profiles must be selected using the lidar data without ancillary data because not all observatories have a surface rain gauge or an equivalent rain or snow detection system. AD-Net uses the color ratio (γ', the ratio of β'_{1064} to β'_{532}) to distinguish rainy and clear (no rain) regions. Large droplets have a large γ' value, so once γ' exceeds a threshold (1.1) over a certain vertical interval in the lower atmosphere, the profile is classified as a rain or snow profile and not used for further analysis of aerosols.

At present, in the AD-Net lidar systems, the overlap of the laser beam and the field of view of the telescope is insufficient for near-field observation. Typically, the full overlap is achieved at around 500 to 600 m altitude. The compensation function $Y(z)$ is therefore inferred from vertical profiles obtained on a day when the planetary boundary layer (PBL) is well developed, when the aerosol distribution is expected to be homogeneous near the surface. $Y(z)$ is determined such that the slope of the compensated signal [$Y(z) \times I_{532}(z)$] is constant near the surface. $Y(z)$ is redetermined after routine maintenance of the lidar equipment is carried out. With this compensation, the optical properties are provided above 120 m altitude. Recently, a small telescope with a wide field of view has been deployed at several lidar observatories in AD-Net, allowing the signal to be measured near the ground (above 60 m altitude). At these observatories, $Y(z)$ can be determined without assuming homogeneous mixing near the surface.

The lidar equation for elastic scattering is resolved into two components (particles and molecules) by the method described by Fernald.[11] The ratio of the extinction coefficient to the backscatter coefficient for aerosols (lidar ratio, S_1) is assumed to be 50 sr. This value was initially determined from
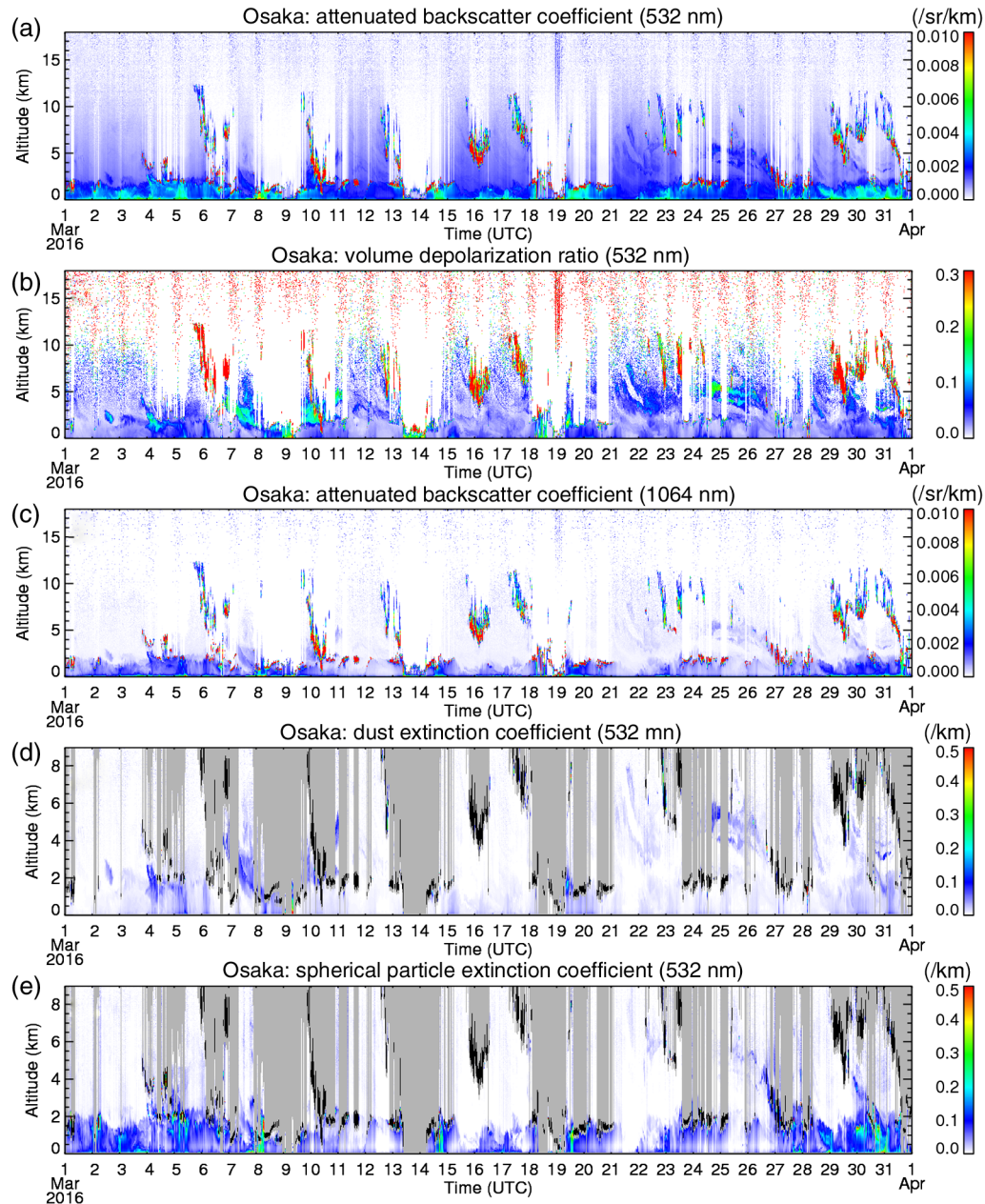
Fig. 3 Examples of time–height sections of (a) attenuated backscatter coefficient at 532 nm (β'_{532}), (b) attenuated backscatter coefficient at 1064 nm (β'_{1064}), and (c) volume depolarization ratio at 532 nm (δv_{532}) and with cloud/rain detection results, (d) dust extinction coefficient at 532 nm (α_{532d}) and (e) spherical particle extinction coefficient at 532 nm (α_{532s}). The observations were made at Osaka in March 2016. The height range for (a)–(c) is from the surface to 18 km and for (d) and (e) is from the surface to 9 km. Black areas in (d) and (e) indicate cloud layers, and gray areas indicate regions above clouds, rain or snow, or no observation data.

values reported in the literature on Asian dust because originally the main target of this lidar network was Asian dust. The vertical profile of molecular densities is obtained from the CIRA-86 global climatology of atmospheric parameters.[12] Usually, the maximum height of Fernald's inversion is set to an altitude of 9 km (6 km before 2012) if the signal-to-noise ratio within that interval is enough to solve the equation. Because 9 km is usually in the troposphere, where the aerosol extinction value is unknown, the lidar equation is first solved with the initial extinction value set to zero. If the resulting aerosol extinction value is negative anywhere between 0 and 9 km height, the extinction

at 9 km is increased slightly and the lidar equation is solved again. Although this method is not rigorous, the obtained extinction is sometimes validated by independent measurements made near the surface or by columnar optical depth observations. Finally, the particulate depolarization ratio (δp_{532}) is calculated from the volume depolarization ratio (δv_{532}) and the particulate backscatter coefficient. These procedures are explained in detail in Ref. 7 and outlined in Fig. 5.

In East Asia, the aerosols being analyzed are assumed to be an external mixture of two components. One component is mineral dust, mainly Asian dust that has been transported a
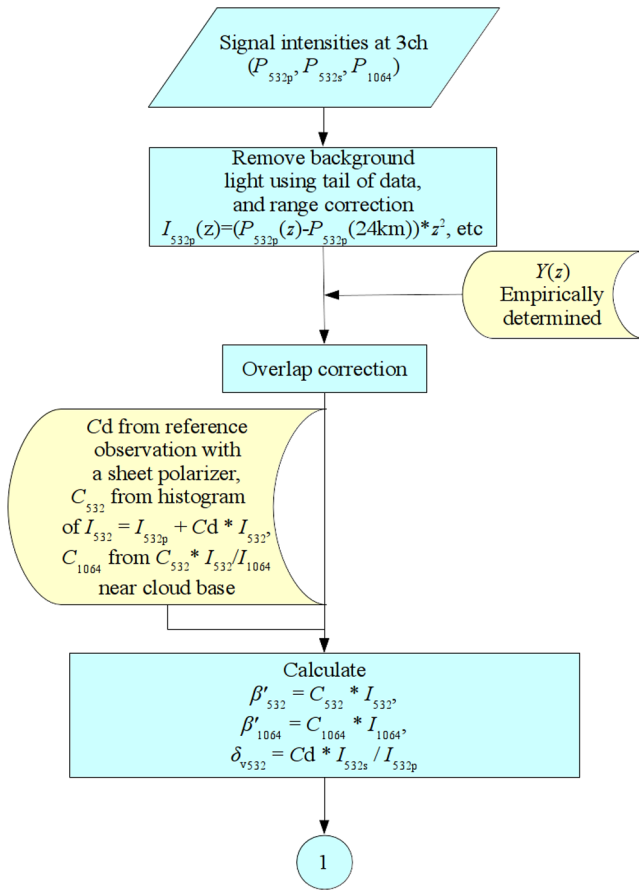
Fig. 4 Flowchart of the backscattering intensities at 532 nm (I_{532}) and at 1064 nm (I_{1064}) calibration procedures.

Fig. 5 Flowchart of the cloud and rain detection procedure and Fernald's inversion.

long distance, which has a particulate depolarization ratio (δp_{532}) of 35%.[7] The other component consists of spherical particles and is assumed to be a mixture of sulfate, nitrate, organic carbon, elemental carbon particles, and sea-salt droplets. The δp_{532} of the latter component is zero because the particles are spherical and Mie scattering theory is applicable. The observed particulate extinction coefficient and particulate linear depolarization values are the linear combination of these two components. Thus, it is possible to use the observed δ_{p532} to separate the total particulate extinction coefficient (α_{532}) into two components, the dust extinction coefficient (α_{532d}) and the spherical particle extinction coefficient (α_{532s}), by calculating the optical dust mixing ratio (R) by following equation:[13]

$$R = \delta_{p532}(1 + 0.35)/\{0.35 \times (1 + \delta_{p532})\}. \quad (3)$$

See Figs. 3(d) and 3(e) for examples of time–height sections of α_{532d} and α_{532s}.

Although β'_{532} was initially estimated from a histogram of all I_{532} data, a more precise estimation is made after inversion. The I_{532} time series at 600 m height is compared with the total backscatter coefficient (sum of molecular backscatter from CIRA-86 and particulate backscatter obtained by inversion) at 600 m height to evaluate the system calibration constant C_{532} again. The revised C_{532} is then utilized to estimate β'_{532} from I_{532}. β'_{1064} is similarly recalculated.
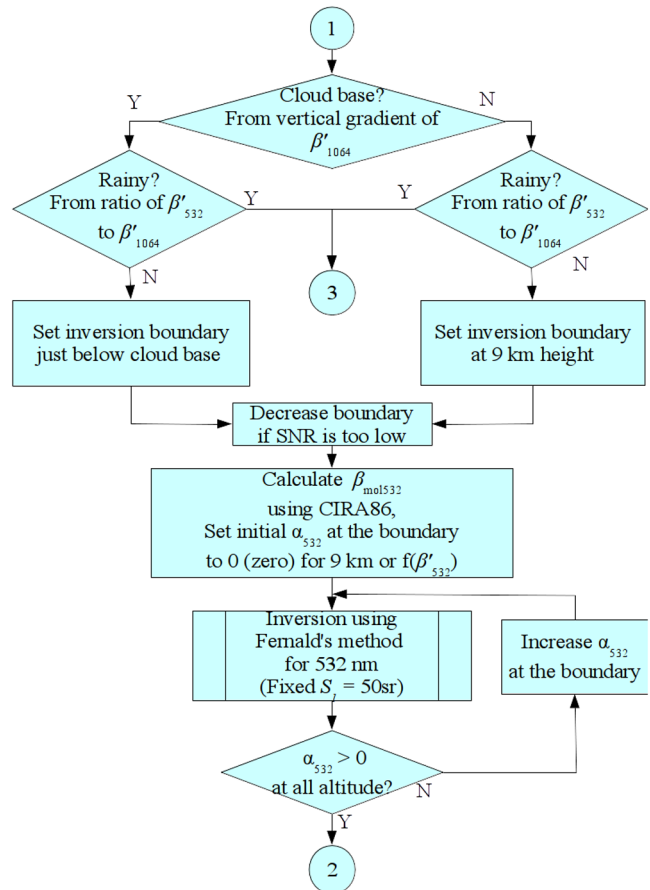
Finally, the AD-Net server generates numerical files in netCDF format that contain time–height sections of β'_{532}, β'_{1064}, δv_{532}, α_{532}, δp_{532}, α_{532d}, and α_{532s}. Quantities below 120 m altitude are eliminated from published data because their reliability is not high owing to the uncertainty of the overlap correction function $Y(z)$. Currently, files are generated hourly for the month and archived one per month. Symbols for two types of missing values (−9999 for cloud layers and −999 for regions above clouds, with rainy or snowy conditions, or with no observations) are embedded into the α_{532}, α_{532d}, and α_{532s}. Simultaneously, figures of time–height sections for these parameters are plotted and both the numerical files and the figures are uploaded onto the AD-Net web page every hour. The procedure is outlined in Fig. 6.

2.4 Validation of Dust Extinction and Comparison with Other Instruments

It is not a simple task to validate dust extinction coefficients obtained by lidar because this parameter cannot be obtained directly by other instruments. However, the surface mass concentration of particles consists mainly of mineral dust during periods with heavy loading of Asian dust. Thus, dust extinction near the surface can be compared with filter-sampled mass concentrations by making some assumptions about vertical mixing near the surface. This comparison was first done in Beijing, China.[13] In Ref. 13, it is reported that the dust extinction coefficient retrieved
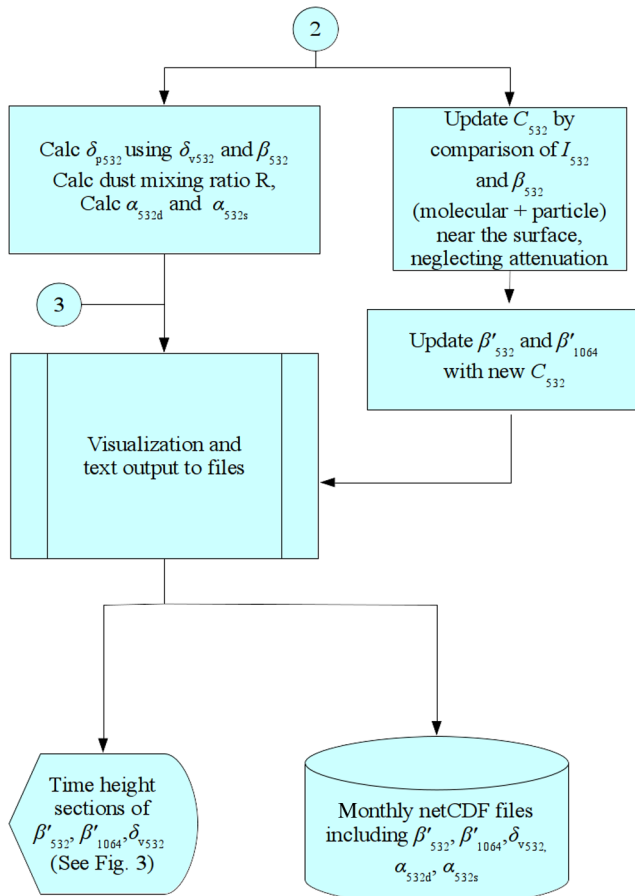
Fig. 6 Flowchart showing the procedures for updating calibration constant (C_{532}) and data recording.

by lidar is almost proportional to the mass concentration of total suspended particles. A similar comparison has been conducted at many stations in Japan during several Asian dust events.[14] In addition, in Ref. [15], the iron concentration in daily PM2.5 samples is compared with the dust extinction coefficient. The results of all these comparisons suggest that dust extinction coefficients determined by lidar are usable as an index of surface dust loading.

2.5 Utilization of the Retrieved Optical Parameters

2.5.1 Use with chemical transport models

A typical use of dust and spherical extinction coefficients is to validate chemical transport models (CTMs). A CTM calculates the four-dimensional distribution of various chemical components (constituent gaseous species and particulates) using meteorological data, emission inventories, chemical reactions, and physical processes (transport, removal, etc.). AD-Net lidar data were first compared with a CTM called CFORS, developed by Kyushu University.[7] To validate CTM results, lidar data should be separated into independent chemical components. Thus, the dust extinction coefficient is useful for validating dust processes in the model. The spherical extinction coefficient is compared with the total extinction due to sulfate, nitrate, organic carbon, elemental carbon, and sea salt.[16,17]

A more sophisticated application of lidar data is to incorporate them into the CTM by assimilation. Data assimilation

is a technique for modifying the aerosol loading in the model in accordance with observed results. In Ref. [18], lidar dust extinction data were assimilated to correct the dust emission factor at the source region of Asian dust in the model. Once dust extinction data have been assimilated, the dust concentration at the surface (PM10) simulated by the model corresponded more realistically to that observed at several observatories in Japan.

2.5.2 Epidemiology of Asian dust

To study the health effects of PM, the mass concentration of particles is usually used as an exposure index. In Japan, environmental standards have been determined for both SPM (suspended PM and almost equivalent to PM6[15]) and PM2.5. However, the chemical components of PM are more important for investigating the actual mechanism of the health effects of the particles. The dust extinction coefficient is suitable for studies of the epidemiology of Asian dust because it captures the quantity of dust continuously. The daily mean α_{532d} value near the surface has been utilized in several epidemiological studies in Japan, some of which found a correlation between health impact and the dust extinction coefficient.[19–23]

2.5.3 Climatology of aerosols

The climatology of aerosols in East Asia can be derived from AD-Net data. Horizontal, seasonal, and interannual variations of extinction coefficients are calculated for each of the two components.

In Fig. 7, mean vertical profiles of dust and spherical particle extinction coefficients are plotted. The exponential decrement with height is apparent in the dust extinction coefficient in most stations; however, a boundary layer structure is found at around 1.8 to 2.3 km in the spherical particle extinction coefficient for many stations. To depict horizontal, annual, and interannual variations of spherical particle extinction coefficients more clearly, the probability density of a time series at a certain height is examined by calculating the 5, 25, 50, 75, and 95 percentiles at the selected height and comparing the results among observatories or among months or years.

The spatial distribution of extinction coefficients of spherical particles among observatories is shown in Fig. 8. An apparent gradient from west to east can be seen except for two stations in Mongolia, but this effect disappears at higher altitudes.

Intra-annual changes differ depending on altitude and among stations. Figure 9 shows monthly percentiles based on data from 2010 to 2015. In the PBL (500 m), seasonal changes are apparent in large cities (Beijing, Seoul, and Tokyo), whereas the annual cycle of changes is different in the lower troposphere (2500 m). These results are consistent with the findings of a comprehensive analysis of anthropogenic particles in this region.[16]

α_{532s} has shown a slight interannual decrease in these cities from 2008 to 2015 (Fig. 10). These results confirm the findings of several studies that have reported a decrease in emissions of anthropogenic gaseous pollutants in this region since 2006.[24]
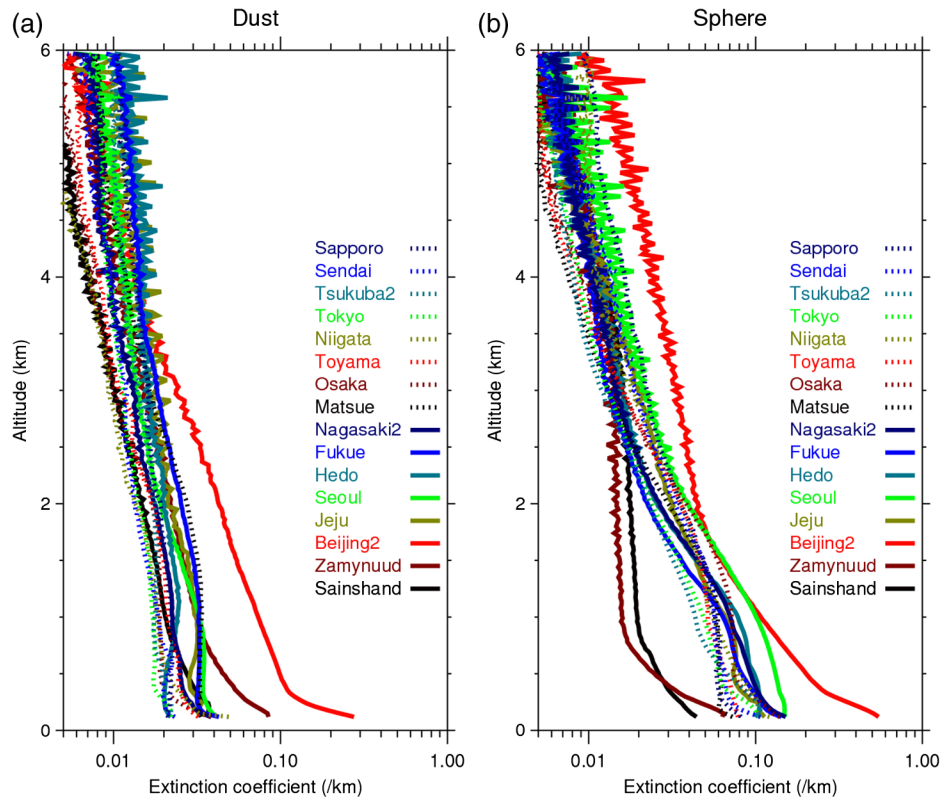
Fig. 7 Averaged vertical profiles of (a) dust extinction coefficient (α_{532d}) during March to May in 2010 to 2015, and (b) spherical particles extinction coefficient (α_{532s}) for all seasons in 2010 to 2015 at 16 stations.

2.5.4 *Qualitative analysis of internal mixtures using the color ratio*

The backscatter signal at 532 nm obtained by AD-Net has been fully utilized for aerosol studies, as shown above. However, the signal at 1064 nm has so far been used in our procedures only to detect rainy and cloudy conditions. Thus, more direct use of the 1064-nm signal for aerosol analysis is a challenge for AD-Net. One example of the utilization of 1064 nm in aerosol studies is related to the internal mixture of dust and anthropogenic particles. If dust with high δp_{532} and γ values is mixed externally with anthropogenic particles with low δp_{532} and γ values, the observed δp_{532} and γ values should reflect the mixture. However, in the real atmosphere, observed δp_{532} and γ values sometimes do not correspond to the values expected for an external mixture. In some cases, lower δp_{532} and higher γ are detected. This implies that the mineral dust particles were chemically modified (e.g., partly deliquesced) and the shapes were modified to be more spherical during the transportation with anthropogenic particles. In such cases, it is possible that dust and anthropogenic particles have become internally mixed.[25,26]

3 Obtaining More Optical Parameters by Multichannel Lidar

We have used $2\beta + 1\delta$ ELs for a long time to monitor aerosols as well as clouds in East Asia and provided mineral dust and spherical aerosol extinctions as well as total aerosol optical properties and cloud base height from the lidar measurements. Lidar measurements with more channels enable providing more detailed information on aerosol optical and microphysical properties and more advanced classification of aerosol components. Thus, we introduced independent extinction measurement by RL and high spectral resolution (HSR) lidar techniques and its multiwavelength measurement to several main observation sites of the AD-Net.

3.1 *Use of Raman Lidar Techniques*

The AD-Net uses the nitrogen RL technique. Details on the RL system, data analysis method, calibration method, measurement uncertainties, and observation results are given in Ref. 27. Here, a summary on the RL observation of AD-Net is given.

We improved the $2\beta + 1\delta$ ELs at five sites of the AD-Net (Tsukuba, Matsue, Fukue, Seoul, and Beijing) by adding a nitrogen Raman scatter measurement channel at 607 nm and have conducted continuous observations since 2009. As a result, this RL system can provide extinction coefficient (α), backscatter coefficient (β), and depolarization ratio (δ) of particles at 532 nm and attenuated backscatter coefficient (β') at 1064 nm. The configuration and specifications are given in Fig. 2(a) and Table 1. Furthermore, we built a multiwavelength RL system (MRL) providing α_{355}, α_{532}, β_{355}, β_{532}, δ_{355}, δ_{532}, and β'_{1064} at Fukuoka, Toyama, and Hedo sites of the AD-Net. The MRL observations started from 2013 at Fukuoka, from 2014 at Hedo, and from 2015 at Toyama. The configuration and specifications are given in Fig. 2(b) and Table 1. For the RL and MRL measurements, we conduct photon-counting measurement for Raman
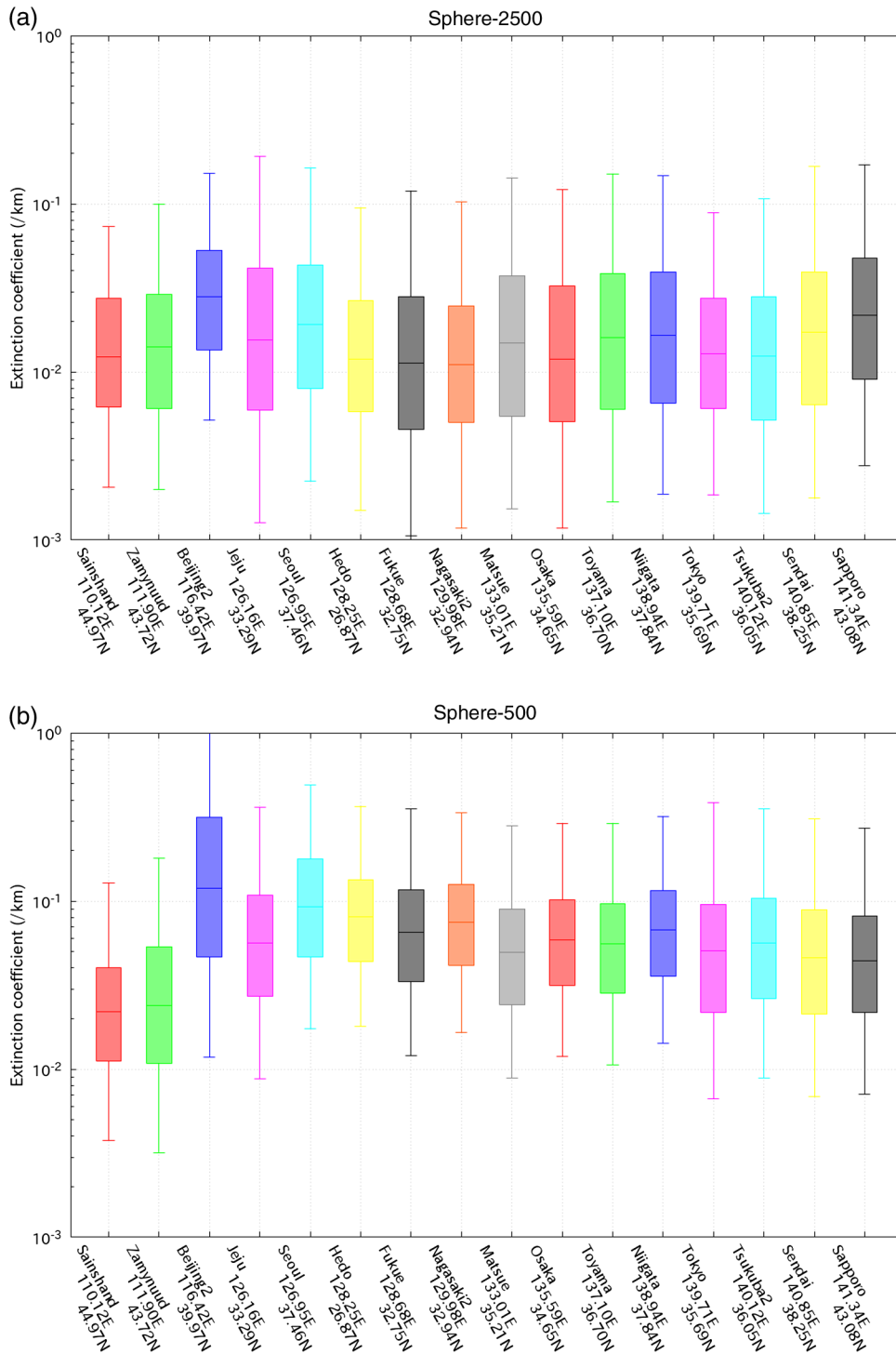
Fig. 8 Distribution of spherical particle extinction coefficients at (b) 500 m altitude and (a) 2500 m altitude among observatories. The boxes and the horizontal line show the 25 to 75 percentile range and the 50 percentile, respectively, and the whiskers show the 5 to 95 percentile range, based on all data collected during 2010 to 2015.

backscatter and analog measurement for elastic backscatter. No Raman channel data are available in the daytime due to strong sunlight.

After reducing signal noises using wavelet transform analysis and moving average, the uncertainties of α, β, δ, and lidar ratio S_1 (α/β) of aerosols in the PBL derived from the RL and MRL measurements are evaluated to be less than 5%, which indicates that the RL and MRL have enough accuracy to understand aerosol optical properties in the PBL.

3.2 Use of High Spectral Resolution Lidar Techniques

The HSR lidar is a more highly sensitive technique than the RL, indicating that the HSR lidar can provide measurements
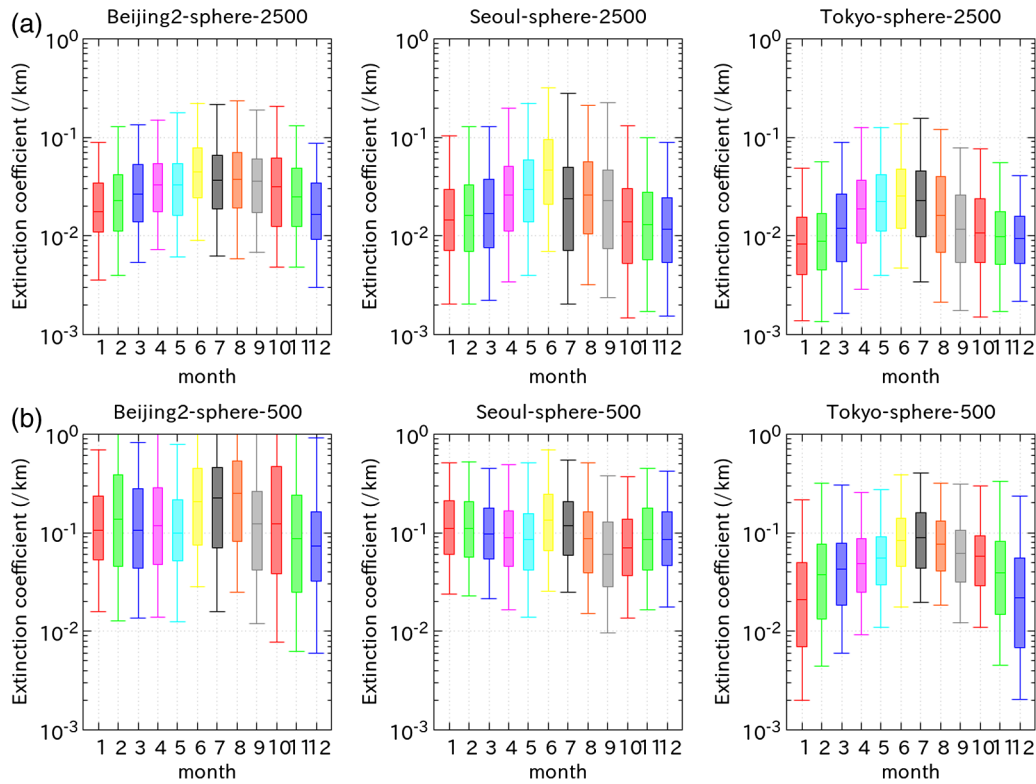
Fig. 9 Same as Fig. 8 but showing monthly variations of the spherical extinction coefficient at (b) 500 m and (a) 2500 m at Beijing, Seoul, and Tokyo, from left to right.
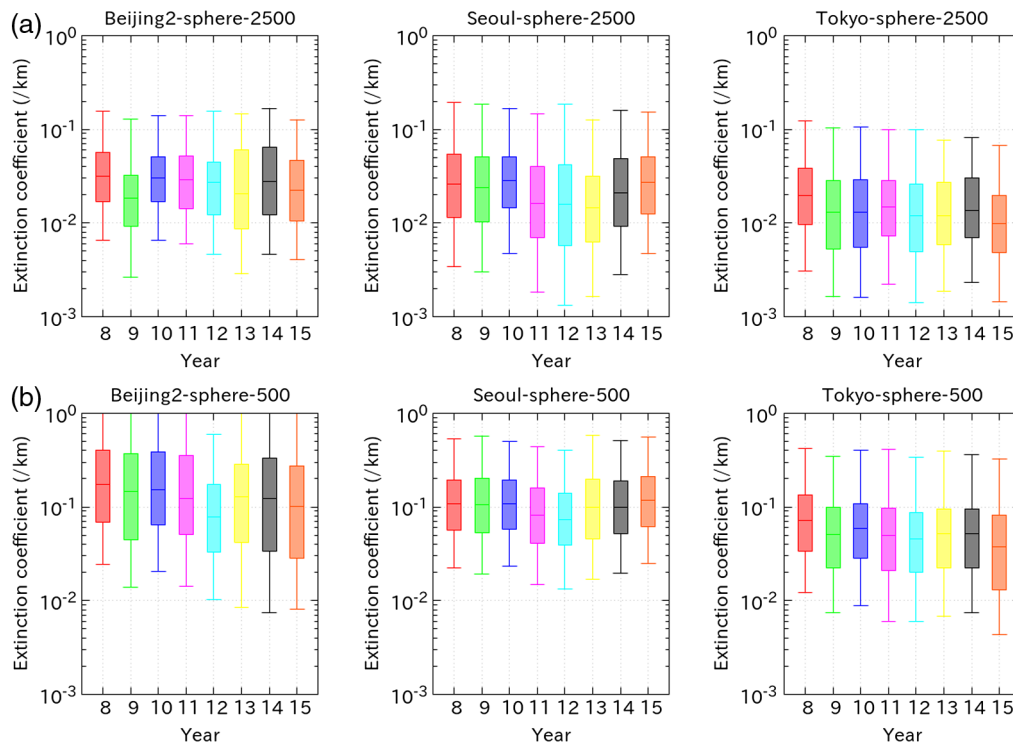

Fig. 10 Same as Fig. 8 but showing year-to-year variations during 2008 to 2015.

with enough signal-to-noise ratio in the daytime as well as the nighttime to retrieve α, β, and δ. We developed a Raman-HSR lidar (RHL) implementing both the nitrogen RL technique at 387 nm and the HSR lidar technique at 532 nm [Fig. 2(c) and Table 1] at the Tsukuba site from 2014. This RHL provides the same products as the MRL (i.e., α, β, and δ at 355 and 532 nm, respectively, and β' at 1064 nm). This system uses the iodine absorption filter[28]

to introduce the HSR lidar technique, indicating that the laser wavelength must be tuned to the center of the iodine absorption line to block the elastic scattering light and transmit the Rayleigh scattering light efficiently. We developed and implemented an automatical feedback control system using two acousto optic modulators[29] to tune the laser wavelength to the absorption line stably for a long period. We conduct photon-counting measurement for Raman backscatter and analog measurement for elastic backscatter including the Rayleigh scatter. No Raman channel data are available in the daytime.

After reducing signal noises in a similar manner as the data analysis of the MRL, the uncertainties of α, β, δ, and S_1 of aerosols in the PBL are evaluated to be comparable to or less than the uncertainties of MRL. Those uncertainties for nighttime are less than half of uncertainties for daytime.

3.3 Aerosol Component Retrieval

A two-component (i.e., mineral dust and spherical particles) algorithm[14] using the EL data was implemented in the standard data processing, and the component products as well as the other products have been provided in public (see Sec. 2.3). Furthermore, as another algorithm using the EL data, we developed a three-component (i.e., mineral dust, sea-salt, and air pollution particles) algorithm[30,31] to estimate a vertical distribution of extinction coefficient for the three aerosol components. This algorithm uses the difference of γ due to particle size and the difference of δ due to particle shape among the aerosol components. For the RL, MRL, and RHL measurements, a four-component (i.e., mineral dust, sea-salt, black carbon, and air pollution particles except black carbon) algorithm[27,32] that further uses the difference of S_1 due to light absorption property among the aerosol components was developed.

The aerosol component products by three- and four-aerosol component algorithms as well as the aerosol and cloud optical property data (i.e., α, β, δ, and S_1) will be made public in the future. Since the developed three- and four-aerosol component retrieval algorithms do not use all the data of MRL and RHL, an aerosol component retrieval algorithm using all the data of MRL and RHL more effectively is being developed to provide more detailed optical and microphysical properties of each aerosol component.

4 Concluding Remarks

Twenty-first century spaceborne lidar (e.g., Ref. 33) covers a wide area of the globe, including oceans and deserts. In contrast, ground-based lidar can cover only the atmosphere above the observatory. However, it can acquire continuous time series of data, and it is useful for monitoring environmental conditions directly related to human populations. Thus, ground-based lidar networks are still very important. In particular, in East Asia, rapid economic growth and changes in environmental protection policy have been significant in several countries. As a result, atmospheric conditions in East Asia can vary greatly. Optical remote sensing is a feasible method for detecting such variation and for detecting emergency conditions, so alerts can be issued for the local inhabitants. Also, data from lidar networks are useful for various types of studies in the field of atmospheric science. AD-Net is now affiliated with GALION [Global Atmosphere Watch (GAW) Lidar Observations

Network], a World Meteorological Organization program. Through GALION, lidar data from around the world are distributed to scientific users such as CTM developers. NIES provides netCDF files of optical properties through its website.

AD-Net will continue to monitor the atmosphere in East Asia and to supply information, including data on optical properties obtained with new technologies, to society. Furthermore, as part of AD-Net observation, we conducted ship-borne lidar measurements using the EL from 1999 to 2015 (e.g., Refs. 34, 35) and using a 532-nm HSR lidar with water–vapor Raman channel at 660 nm in 2011 (e.g., Refs. 36, 37) in corroboration with the Japan Agency for Marine-Earth Science and Technology (JAMSTEC). The MRL with water-vapor Raman scattering detection channel (660 nm) has been used since 2015. It is essential for observing temporal and spatial distributions of aerosols and clouds and their optical and microphysical properties over land and ocean to understand and evaluate global environmental change.

References

1. Intergovernmental Panel on Climate Change, *Intergovernmental Panel on Climate Change*, Cambridge University Press (2014).
2. International Agency for Research on Cancer, *Air Pollution and Cancer*, World Health Organization (2013).
3. G. Pappalardo et al., "EARLINET: towards an advanced sustainable European aerosol lidar network," *Atmos. Meas. Tech.* **7**, 2389–2409 (2014).
4. J. R. Levis et al., "Overview of MPLNET version 3 cloud detection," *J. Atmos. Oceanic Technol.* **33**, 2113–2134 (2016).
5. J. L. Guerrero-Rascado et al., "Latin American Lidar Network (LALINET) for aerosol research: diagnosis on network instrumentation," *J. Atmos. Sol. Terr. Phys.* **138**–**139**, 112–120 (2016).
6. J. H. Seinfeld et al., "ACE-ASIA: regional climatic and atmospheric chemical effects of Asian dust and pollution," *Bull. Am. Meteorol. Soc.* **85**, 367–380 (2004).
7. A. Shimizu et al., "Continuous observations of Asian dust and other aerosols by polarization lidars in China and Japan during ACE-Asia," *J. Geophys. Res.* **109**, D19S17 (2004).
8. T. Murayama et al., "An intercomparison of lidar-derived aerosol optical properties with airborne measurements near Tokyo during ACE-Asia," *J. Geophys. Res.* **108**, 8561 (2004).
9. Y. Iwasaka et al., "Transport of Asian dust (KOSA) particles; importance of weak KOSA events on the geochemical cycle of soil particles," *Tellus* **35B**, 189–196 (1988).
10. V. Freudenthaler et al., "Depolarization ratio profiling at several wavelengths in pure Saharan dust during SAMUM 2006," *Tellus* **61**, 165–179 (2009).
11. F. G. Fernald, "Analysis of atmospheric lidar observations—some comments," *Appl. Opt.* **23**(5), 652–653 (1984).
12. Committee on Space Research; NASA National Space Science Data Center, *COSPAR International Reference Atmosphere (CIRA-86): Global Climatology of Atmospheric Parameters*, NCAS British Atmospheric Data Centre (2006).
13. N. Sugimoto et al., "Record heavy Asian dust in Beijing in 2002: observations and model analysis of recent events," *Geophys. Res. Lett.* **30**, 1640 (2003).

14. A. Shimizu et al., "Relationship between lidar-derived dust extinction coefficients and mass concentrations in Japan," *Sci. Online Lett. Atmos.* **7A**, 1–4 (2011).
15. N. Kaneyasu et al., "Comparison of Lidar-derived dust extinction coefficients and the mass concentrations of surface aerosol," *J. Jpn. Soc. Atmos. Environ.* **47**, 285–291 (2012).
16. Y. Hara et al., "Seasonal characteristics of spherical aerosol distribution in eastern Asia: Integrated analysis using ground/space-based lidars and a chemical transport model," *Sci. Online Lett. Atmos.* **7**, 121–124 (2011).
17. D. Goto et al., "An evaluation of simulated particulate sulfate over East Asia through global model intercomparison," *J. Geophys. Res.* **120**, 6247–6270 (2015).
18. K. Yumimoto et al., "Adjoint inversion modeling of Asian dust emission using lidar observations," *Atmos. Chem. Phys.* **8**, 2869–2884 (2008).
19. K. Ueda et al., "Long-range transported Asian dust and emergency ambulance dispatches," *Inhalation Toxicol.* **24**, 858–867 (2012).
20. K. Kanatani et al., "Effect of desert dust exposure on allergic symptoms: a natural experiment in Japan," *Ann. Allergy, Asthma Immunol.* **116**(5), 425–430 (2016).
21. T. Higashi et al., "Effects of Asian dust on daily cough occurrence in patients with chronic cough: a panel study," *Atmos. Environ.* **92**, 506–513 (2014).
22. M. Watanabe et al., "Association of sand dust particles with pulmonary function and respiratory symptoms in adult patients with asthma in western Japan using light detection and ranging: a panel study," *Int. J. Environ. Res. Public Health* **12**(10), 13038–13052 (2015).
23. S. Kashima et al., "Asian dust and daily all-cause or cause-specific mortality in western Japan," *Occup. Environ. Med.* **69**, 908–915 (2012).
24. Z. Lu et al., "Sulfur dioxide emissions in China and sulfur trends in East Asia since 2000," *Atmos. Chem. Phys.* **10**, 6311–6331 (2010).
25. N. Sugimoto et al., "Observation of dust and anthropogenic aerosol plumes in the Northwest Pacific with a two-wavelength polarization lidar on board the research vessel Mirai," *Geophys. Res. Lett.* **29**, 71–74 (2002).
26. N. Sugimoto et al., "Detection of internally mixed Asian dust with air pollution aerosols using a polarization optical particle counter and a polarization-sensitive two-wavelength lidar," *J. Quant. Spectrosc. Radiat. Transfer* **150**, 107–113 (2015).
27. T. Nishizawa et al., "Ground-based network observation using Mie-Raman Lidars and multi-wavelength Raman lidars and algorithm to retrieve distributions of aerosol components," *J. Quant. Spectrosc. Radiat. Transf.* (2016).
28. Z. Liu, I. Matsui, and N. Sugimoto, "High-spectral-resolution lidar using an iodine absorption filter for atmospheric measurements," *Opt. Eng.* **38**, 1661–1670 (1999).
29. T. Nishizawa, N. Sugimoto, and I. Matsui, "Development of a dual-wavelength high-spectral-resolution lidar," *Proc. SPIE* **7860**, 78600D (2010).
30. T. Nishizawa et al., "An algorithm that retrieves aerosol properties from dual-wavelength polarization lidar measurements," *J. Geophys. Res.* **112**, D06212 (2007).
31. T. Nishizawa et al., "Algorithm to retrieve aerosol optical properties from two-wavelength backscatter and one-wavelength polarization lidar considering nonsphericity of dust," *J. Quant. Spectrosc. Radiat. Transfer* **112**, 254–267 (2011).
32. T. Nishizawa et al., "Algorithm to retrieve aerosol optical properties from high-spectral-resolution lidar and polarization Mie-scattering lidar measurements," *IEEE Trans. Geosci. Remote Sens.* **46**, 4094–4103 (2008).
33. D. M. Winker et al., "Overview of the CALIPSO mission and CALIOP data processing algorithms," *J. Atmos. Oceanic Technol.* **26**, 2310–2323 (2009).
34. N. Sugimoto et al., "Latitudinal distribution of aerosols and clouds in the western Pacific observed with a lidar on board the research vessel Mirai," *Geophys. Res. Lett.* **28**, 4187–4190 (2001).
35. T. Nishizawa et al., "Aerosol retrieval from two-wavelength backscatter and one-wavelength polarization lidar measurement taken during the MR01K02 cruise of the R/V Mirai and evaluation of a global aerosol transport model," *J. Geophys. Res.* **113**, D21201 (2008).
36. J. Suzuki et al., "The occurrence of cirrus clouds associated with eastward propagating equatorial n=0 inertio-gravity and Kelvin waves in November 2011 during the CINDY2011/DYNAMO campaign," *J. Geophys. Res.* **118**, 12, 941–12, 947 (2013).
37. H. Bellenger et al., "Observation of moisture tendencies related to shallow convection," *J. Atmos. Sci.* **72**, 641–659 (2015).

Atsushi Shimizu is a senior researcher at the National Institute for Environmental Studies (NIES), Japan. He received his BS degree from the Science Faculty, Kyoto University, in 1994 and his MS degree and PhD in atmospheric physics from the Graduate School of Science, Kyoto University, in 1996 and 1999, respectively.

Tomoaki Nishizawa received his BS, MS, and DSc degrees in geophysics from Tohoku University, Japan, in 1999, 2001, and 2004, respectively. He has worked for NIES, Japan since 2007 and is currently a head of the Advanced Remote Sensing Section of NIES. His research field is related to atmospheric environment and climate. He is engaged in aerosol and cloud observation using lidars and development of lidar systems and data analysis methods.

Yoshitaka Jin is a research associate of the NIES, Japan. He received his DSc degree from Nagoya University in 2014. Since 2009, he has conducted research on aerosol optical properties with active remote sensing. His current research covers the development of high-spectral-resolution lidar methods and applications of ceilometer for aerosol measurement. He is a member of the Japan Association of Aerosol Science and Technology, and the Meteorological Society of Japan.

Sang-Woo Kim is an associate professor of the School of Earth and Environmental Sciences, Seoul National University, Republic of Korea. He received his PhD in atmospheric sciences from Seoul National University in 2005 and has conducted research on the monitoring of air pollutants and atmospheric aerosols and evaluating their climate effects based on ground-based and airborne *in situ* and active optical remote sensing measurements.

Wang Zifa: Biography is not available.

Batdorj Dahdondog is a senior officer of the National Agency for Meteorology and Environmental Monitoring of Mongolia (NAMEM). He received his master's degree from the National University of Mongolia in 2005. Since he joined the Institute of Meteorology and Hydrology (IMH) in 2003. He has conducted various research in the climatology and environmental field.

Nobuo Sugimoto is a fellow of NIES, Japan. He received his DSc degree in laser spectroscopy from the University of Tokyo in 1985. Since he joined NIES in 1979, he has conducted various research on the development and applications of active optical remote sensing methods, including differential absorption lidars, high-spectral-resolution lidars, and ground-based networks of lidars. He is a member of SPIE and a senior member of OSA.